IEEE Access
Multidisciplinary | Rapid Review | Open Access Journal

Received 18 May 2024, accepted 10 June 2024, date of publication 13 June 2024, date of current version 28 June 2024.

Digital Object Identifier 10.1109/ACCESS.2024.3414169

RESEARCH ARTICLE

Hybrid Compensation Based Efficient Wireless Charging System Design With Solar Photovoltaic Interface Toward Sustainable Transportation

K. ARULVENDHAN[1], SRINIVAS KANDADAI NAGARATNAM[1], R. NARAYANAMOORTHI[2], MOHAMMED ALHARBI[3], AND SEADA HUSSEN[4]

[1]Department of Electrical and Electronics Engineering, SRM Institute of Science and Technology, Ramapuram Campus, Chennai, Tamil Nadu 600089, India
[2]Department of Electrical and Electronics Engineering, SRM Institute of Science and Technology, Kattankulathur, Tamil Nadu 603203, India
[3]Department of Electrical Engineering, College of Engineering, King Saud University, Riyadh 11421, Saudi Arabia
[4]Department of Electrical Power, Adama Science and Technology University, Adama 1888, Ethiopia

Corresponding authors: K. Arulvendhan (arulvenk@srmist.edu.in), R. Narayanamoorthi (narayanamoorthi.r@gmail.com), and Seada Hussen (seada.hussen@aastu.edu.et)

This work was supported in part by the Researchers Supporting Project, King Saud University, Riyadh, Saudi Arabia, under Grant RSP2024R467; and in part by the Government of India, Department of Science and Technology (DST) Science and Engineering Research Board (SERB) Core Re-Search under Grant CRG/2020/004073.

ABSTRACT The adoption of wireless charging for Electric Vehicles (EVs) is on the rise, promising enhanced user convenience. Concurrently, there is a pressing need for increased integration of renewable energy into the transportation sector to mitigate greenhouse gas emissions. However, wireless charging systems face challenges such as power transfer fluctuations under load and variations in coupling coefficients. This research introduces a novel solution: a Photovoltaic (PV)-integrated hybrid-compensated wireless charging system tailored for EV applications. The study addresses critical hurdles in achieving optimal efficiency and power delivery while accommodating significant misalignments inherent in Wireless Power Transfer (WPT) systems, particularly beneficial for EV charging. Compared to conventional compensation WPT systems, the proposed hybrid compensation approach significantly enhances transfer efficiency and reduces system current stress. The paper proposes the utilization of S-LCC/SP-compensated constant current (CC) and constant voltage (CV) system for PV-integrated static WPT systems. Experimental validation of the proposed system is conducted on a 3.3-kW laboratory-scale prototype. The findings demonstrate consistent power transfer across a 100–200 mm air gap, maintaining an efficiency of 91.3%. These results confirm the effectiveness of the proposed system in real-world applications.

INDEX TERMS Electric vehicle charging, photovoltaic integration, S-SP/LCC resonant network, wireless charging.

I. INTRODUCTION

Rapid population and industrial growth results in a shortage of traditional energy sources. This scarcity drives researchers to focus on alternative energy sources including renewable and non-renewable energy sources. The renewable energy sources are attracted among the community due to the global warming issues and CO_2 emission [1], [2]. Among the various renewable energy sources, the solar photovoltaic (PV) sources offer significant advantages over others [3]. The transportation sector is the largest consumer of energy among human activities [4], [5]. The introduction of electric vehicles (EVs) has marked significant progress in transportation research. Since the invention of galvanic cell-powered electric cars in 1837, the technology for EV battery charging has been continually refined over the centuries [6], [7]. Due to their inherent benefits, such as zero pollution, increased energy efficiency, and decreased noise

The associate editor coordinating the review of this manuscript and approving it for publication was Shuo Sun.

levels, electric cars are becoming a competitive alternative to conventional gasoline-powered internal combustion engine vehicles (ICEVs) [8], [9]. The limited driving range imposed by battery capacity is a fundamental practical barrier to their promotion and prevents EVs from being widely adopted [10], [11]. To hasten the commercialization of these environmentally friendly automobiles, urgent attention is needed to establish effective EV charging infrastructures. Traditionally, conductive charging has involved connecting an EV to the power grid using a cable [12]. This approach presents difficulties because it calls for heavy gauge cables that are difficult to handle and could leak electrical current [13]. On the other side, WPT technology is a modern and well-liked substitute for conductive charging [14]. WPT provides a fully automated, convenient, intelligent, safe, and superior charging experience compared to cable charging [15], [16]. The field of WPT solutions for EVs has seen a substantial increase in the interest in inductive power transfer (IPT). The PV and WPT systems are most likely to be used in public and private parking spaces with the roof top solar PV and installed WPT system. Moreover, using the WPT technique the charging process can be automated based on the availability of the solar PV system. Which is the crucial factor to enhance the installation of the PV modules in the EV charging station and the integration [17], [18].

Due to the sensitivity of power transmission and efficiency to changes in the coupling coefficient, WPT systems necessitate accurate alignment of the transmitter and receiver coils [19], [20]. Similarly, the changes in vehicle types and parking locations, achieving a constant coupling coefficient in actual applications is impossible. In contrast to conventional WPT applications, it can be difficult and depends on the driver and the surroundings to align the transmitter and receiver in EV WPT systems [21]. As a result, researchers are working to increase the EV wireless charging systems' misalignment tolerance using different approaches [22], [23]. Innovations in the charge couplers, resonant networks, and high-frequency power converters are the main elements to address the misalignment in the wireless charging system. Based on flux orientation, charging couplers are divided into non-polarized pads for 1-D (vertical) flux generators and polarized pads for 2-D (vertical and horizontal) flux generators [24], [25]. Non-polarized pad shapes include those that are circular, square, rectangular, and hexagonal; polarized pad forms include those that are double-D shaped, quadrature, and bipolar. Polarized pads are made for dynamic charging systems, whilst non-polarized pads are best suited for stationary charging applications [26], [27]. High-frequency power inverters make it easier for charging couplers to be activated and deactivated. On the other side, Numerous strategies have been put up to overcome this issue to guarantee steady energy transmission despite changes in coupling conditions [28]. The three main types of these techniques are impedance matching, phase shift or variable frequency adjustments, and dc-dc converters [29], [30]. These methods do have certain disadvantages, though, like high costs, poor efficiency, and complicated system controls. The system is made even more difficult by the fact that dual-side wireless communication between the transmitter and receiver is frequently considered necessary for feedback control [30]. A dependable WPT system that is symmetric circuit-based and using Parity-Time (PT) has just been unveiled [31], [32]. Power for this PT-based system comes from a negative resistor, which differs from a typical resistor in that when an associated reference direction is selected, the current through the negative resistor flows in the opposite direction of its voltage [33], [34]. This configuration creates a fine energy balance in the precise PT-symmetric zone and automatically maintains it in the strong coupling region. As a result, the system operates without dual-side communication and maintains constant efficiency and power even when the coupling coefficient varies. The load conditions outlined in earlier publications [35] and [36] presuppose constancy, which might not line up with the dynamic needs of battery charging. While variations in load resistance are considered in [37] and [38], adding a dc-dc converter at the inverter's front end is the solution to maintain a constant output power. This suggested solution is also restricted to the PT-symmetric zone and add additional difficulties when the battery's equivalent load resistance rises and inevitably disturbs the PT-symmetric conditions.

Furthermore, the Constant Current/Constant Voltage (CC/CV) charging for battery applications is only briefly explored and analyzed in the existing PT-based WPT systems [39], [40], which primarily focus on output power changes. On the other hand, the hybrid compensation methods are showing better performance with simple control approach on the WPT system under varying load and misaligned conditions [41], [42]. Different compensation techniques are explored in the literature for the WPT applications to minimize the VA rating of the charger [43], [44]. Likewise, the use of hybrid compensation techniques for the WPT system are explored to achieve the CC and CV mode of operation. The dual side LCC, LCC-S and S-SP topologies are also studied to get the CC/CV operation independent of the load variation [45], [46]. However, most of these techniques require complex control mechanisms or receiver side communication modules. Meanwhile, the PV integrated wireless charging station offers flexible control over adjusting the power at the receiver side, by varying the DC-DC converter employed at the input of the high frequency inverter. Only limited concentrations are provided on the PV integrated WPT system with hybrid compensation techniques for achieving the load independent CC and CV mode of operation [47], [48]. The integration of PV with the WPT system using hybrid compensation provides direct advantage of making the system more load independent in nature. Particularly the use of receiver side DC-DC converter is eliminated, and the CC/CV control is achieved with the proposed technique. Hence, this manuscript proposes a PV

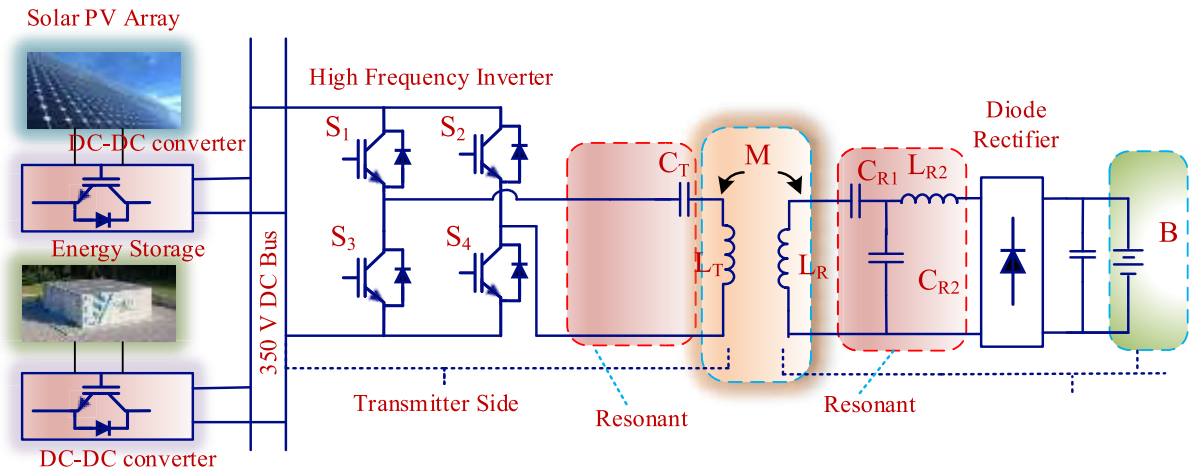

FIGURE 1. Functional diagram of PV integrated wireless charging system.

integrated hybrid compensation topology based wireless charging system for EV applications to provide CC and CV mode of operation. The major contribution of the proposed work is as follows:

- The use of receiver side-controlled S-LCC/SP network for the Wireless Charging System to obtain CC and CV mode of operation.
- Analysis and design of the PV integrated Wireless charging system with CC and CV regulation.
- The simulation analysis of the proposed system under different coupling points, load conditions, CC and CV conditions are analyzed.
- The simulation and experimental validation of the proposed method for 3.3 kW rating and 85 kHz operating frequency.

This manuscript's section II offers a thorough examination of how the proposed PV integrated WPT system operates. It briefly discusses the topologies of the S-LCC/SP based hybrid compensation network, the positioning of charging couplers, and the PV integrated DC-DC converter for the CC and CV mode of operation. Section III follows with a thorough evaluation of the experimental configuration for the proposed charging system. Incorporating experimental waveforms, this section provides a brief analysis of the S-SP and S-LCC modes and demonstrates the delivery of CC and CV profiles. Finally, in Section IV, the paper draws to a close its examination of the suggested work by highlighting its shortcomings and identifying prospective directions for further exploration.

II. PV INTEGRATED WIRELESS CHARGING SYSTEM WITH HYBRID COMPENSATION

Electricity generated by solar PV systems is used as an extra power source for EV charging stations. By using this strategy, carbon emissions from traditional fossil-fueled power plants are reduced. In essence, PV power can be used to charge EVs when the traditional grid supply is unavailable, reducing dependency on non-renewable energy sources. Additionally, adding PV generation and Vehicle-to-Grid (V2G) technologies to the system can lower peak load requirements and improve microgrid stability [49]. It's important to understand that EVs differ from conventional energy storage devices in that they are mobile. For instance, a significant number of EVs may need to be present at the charging station in order for V2G to be implemented. Even while V2G is essential for reducing peak power consumption or improving microgrid stability, its effectiveness may be limited by the quantity of EVs present at any given time. Therefore, it is crucial to comprehend and take into account these unique qualities of a PV-powered EV charging station when using it as a way to improve microgrid stability.

The layout of the Wireless EV charging station powered by solar energy is shown in Figure 1. The station includes inverters, EVs, wireless charge couplers, PV arrays, and DC/DC converters. The high frequency inverter, which controls power transmission between the charging station and the coupler, is an essential component. Local loads are connected in parallel between the microgrid and the inverter. The PV array produces energy to power local loads, the grid, and EV charging system. Using a DC/DC converter with maximum power point tracking (MPPT), the PV array's power harvesting is optimized. Through the wireless charge coupler and high frequency inverter and rectifier the charging process takes place to the EV. The essential modules of the proposed charging system are PV integrated D.C. bus, High frequency inverter, S-LCC/SP resonant network, and DD charging couplers.

A. PV INTEGRATED CHARGING SYSTEM

The PV power in maximum power point tracking (MPPT) mode is represented by P_{PVM} in the energy management system, whereas P_{PV} stands for the total PV power. Additionally,

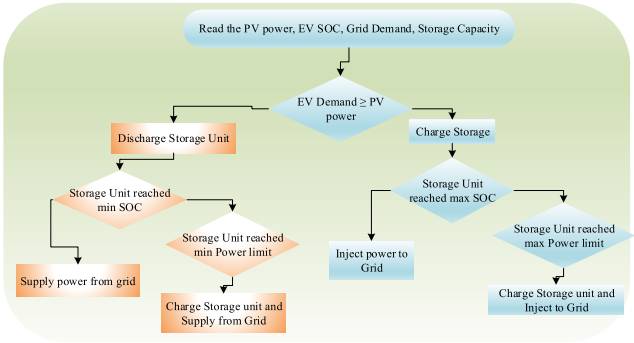

FIGURE 2. Energy management of PV integrated WPT system.

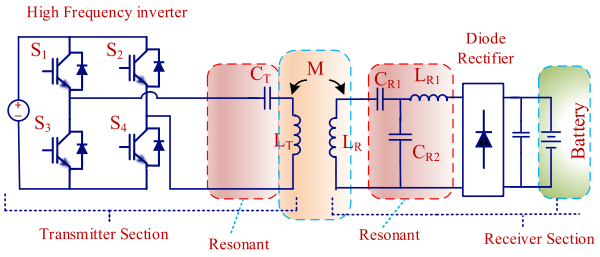

FIGURE 3. Equivalent circuit of wireless charging system.

P_{EVD} reflects the overall power demand from EVs, while P_{EV} designates the total power consumed by all EVs. P_G stands for electricity from the public grid. P_S is for stationary storage power. Power can be supplied or absorbed by the public grid. A capacitor C acts as a common DC bus in the arrangement, linking the charging station's parts via special converters. To extract power that has been MPPT-optimized from PV sources, a DC/DC converter is used to connect them to the DC bus. Through a reversible DC/DC converter, the stationary storage, which is necessary for building the DC microgrid, is connected. A DC/DC converter connects the DC load, which is symbolized by the batteries of EVs. A three-phase bidirectional AC/DC converter connects to the public grid to provide a constant power supply and manage the power gap between production and demand. The stationary storage can discharge power to the common DC bus and is only charged by PV sources [50], [51]. Figure 2 shows the energy management approach is organized hierarchically as follows: The stationary storage is used as a backup energy source after PV, which serves as the major energy source for EV charging. The last recourse for charging EVs is the public grid. Notably, when the stationary storage reaches its maximum limits in terms of power or state of charge, excess energy from PV sources and the public grid are used to charge the store.

A DC microgrid is at the heart of the architecture of the PV-powered charging station, as shown in Figure 1. Thus, maintaining the power balance is crucial, as suggested by [52], [53].

$$P_{PV}(t_k) = P_S(t_k) + P_G(t_k) + P_{EV}(t_k) \tag{1}$$

where, $t_k = t_i, t_i + \nabla t, t_i + 2\nabla t, t_i + 3\nabla t \ldots$, the generated PV power calculated during MPPT mode of operation is

$$P_{PVM}(t_k) = P_{PV}(t_k)\left(\frac{g(t_k)}{1000}\right)(\gamma(T_{PV}(t_k) - 25) + 1)N_{PV} \tag{2}$$

For the sake of convenience, equation (3) uses a condensed description of the state of charge for the stationary storage, abbreviated as SOC [54], [55]. Self-discharge and temperature effects are not considered in this model, whereas overcharging/discharging protections are described by equation (5).

$$SOC(t_k) = SOC(t_0) + \frac{1}{3600\,E_S}\int_{t_0}^{t_k} P_S(t_k)\,dt \tag{3}$$

$$SOC_{min} \le SOC(t_k) \le SOC_{max} \tag{4}$$

$$P_{Smin} \le P_S(t_k) \le P_{Smax} \tag{5}$$

Energy from PV sources, stationary storage, and the grid collectively contributes to charging EVs. The allocation of these energies is determined through the formula as

$$E_{PV} = \int_{t_a}^{t_d} P_{PV}(t_k)\frac{P_{EVD}(t_k)}{P_{EV}(t_k)}dt_k \tag{6}$$

$$E_G = \int_{t_a}^{t_d} P_G(t_k)\frac{P_{EVD}(t_k)}{P_{EV}(t_k)}dt_k \tag{7}$$

$$E_S = \int_{t_a}^{t_d} P_S(t_k)\frac{P_{EVD}(t_k)}{P_{EV}(t_k)}dt_k \tag{8}$$

B. HYBRID COMPENSATED WIRELESS CHARGING SYSTEM

Figure 3 shows a schematic representation of the proposed hybrid compensated WPT system. It has a full-bridge inverter with four power switches (S_1–S_4) that transform direct current voltage (V_{dc}) from the DC bus into alternating current square voltage (V_{ac}). Two coils, L_T and L_R, with mutual inductance M_{TR} connect the transmitter and receiver parts. The tuning capacitors C_T and C_R are connected on the transmitting and receiving sides, respectively. The letters R_T and R_R stand for the transmitter's and receiver's internal resistances, respectively. A filter capacitor with capacitance C_f and the rectifier diodes D_1–D_4 performs important functions. A short-circuit switch, S, is also included and is temporarily triggered before the start of charging. Currents I_T and I_R, which flow through the transmitting and receiving coils, respectively. The equivalent resistance of the rectifier is indicated by the letters R_L, while V_R stands for the rectifier's input voltage. Finally, I_o and V_o are the dc output voltage and current, respectively. It is simple to derive the equations for the fundamental elements of voltage and current, V_{ac}, V_R, I_T, and I_R, in terms of the phasors V_T, V_R, I_T, and I_R as given from (9) to (12).

$$V_T = \frac{2\sqrt{2}}{\pi}V_{dc}\sin(0.5D\pi) \tag{9}$$

$$I_R = \frac{\pi\sqrt{2}}{4} I_0 \tag{10}$$

$$V_R = \frac{2\sqrt{2}}{\pi} V_0 \tag{11}$$

$$R_L = \frac{8}{\pi^2} R_B \tag{12}$$

The parameters of the designed WPT system are calculated from the load resistance value, output power, load voltage, input PV voltage.

C. CONSTANT CURRENT AND CONSTANT VOLTAGE HYBRID COMPENSATION NETWORK

The loosely linked coil topologies and misalignment problems are frequent challenges encountered when implementing an WPT system. These difficulties increase the leakage inductance between the coils, which lowers the system's capacity for power transfer and overall effectiveness. However, a workable method to address these issues is to successfully use passive resonant networks for reactive power compensation. The system can considerably increase its ability to transfer maximum power by compensating the reactive power [56], [57]. In this paper, a hybrid resonant receiver-side network structure with constant voltage and constant current is presented. A change in the mode of operation is made possible by the anti-parallel auxiliary switch, which strategically connects and disconnects the series compensating inductor. A series compensation using a single capacitor is used on the transmitter side to reduce the number of passive components and improve resistance to load changes and misalignment. The corresponding S-LCC and S-SP network circuits are shown in Figures 4(a) and (b). Figure 4(a) shows the CC mode of operation with the ASW switch at the receiver side is disconnected from the inductor and the network supply constant current when the input is of voltage. In Figure 4(b), the ASW switch is connected to the circuit and turned to ON state which bypasses the inductor. Hence, the network will maintain the output voltage as constant irrespective of the load variation. Equations (5)– (9) must hold true for constant current delivery in the S-LCC network. The CC mode increases the WPT system's effectiveness while simultaneously extending battery life.

Considering the following assumptions for simplification

$$j\omega L_T + \frac{1}{j\omega C_T} = jX_{LT} - jX_{CT} = jX_T \tag{13}$$

$$j\omega L_R + \frac{1}{j\omega C_R} = jX_{LR} - jX_{CR} = jX_R \tag{14}$$

$$\frac{1}{j\omega C_R} = -jX_{CR2} \tag{15}$$

$$j\omega L_f = jX_{LR1} \tag{16}$$

$$j\omega M = jX_M \tag{17}$$

The cascaded design of the LC network guarantees steady current delivery to the charging device. The charging system maintains a steady rated current while progressively raising it when the battery voltage is below the rated value.

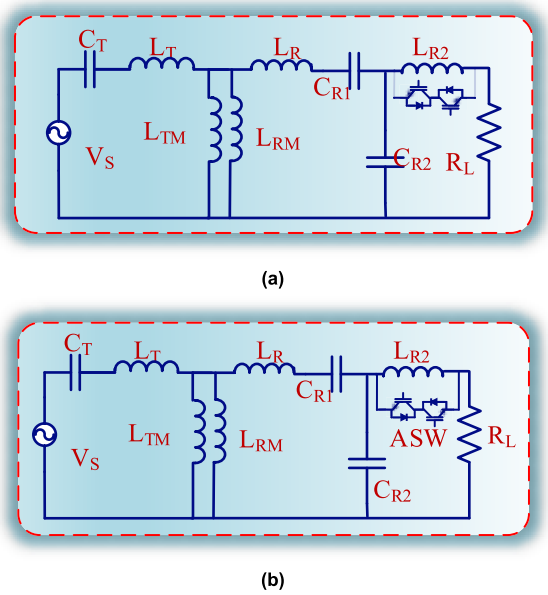

FIGURE 4. Equivalent circuit modes (a) CC mode of operation (b) CV mode of operation.

When the battery voltage reaches the designated value, the auxiliary switch shuts and disconnects the inductor. As a result, the voltage delivered by the charging network is constant, although the current rapidly degrades. Equations (12) through (17), calculation of the total impedance of the S-SP network, must be satisfied for constant voltage to occur in S-SP networks. The T-network ensures that the charging system receives continuous voltage delivery. The admittance gain of the S-LCC network is expressed as

$$G_{VI} = \frac{I_R}{V_R} = \frac{\pi^2 I_B}{8E} \tag{18}$$

The mutual inductance of the circuit is given as

$$M = \frac{8E}{\pi^2 I_B \omega} \tag{19}$$

The voltage gain of the circuit is expressed as

$$G_{VV} = \frac{V_R}{V_T} = \left| \frac{-X_S}{X_M} \right| \tag{20}$$

The receiver side compensation capacitance is given as follows

$$C_R = \frac{\pi^2 I_R}{\omega(\pi^2 \omega L_R I_R + 8V_R)} \tag{21}$$

During the CC mode and CV mode of operation of the circuit, the compensation capacitance is given as

$$C_{T-CC} = \frac{1}{\omega^2 L_T} \tag{22}$$

$$C_{T-CV} = \frac{\pi^2 I_R V_R}{\omega(\pi^2 \omega V_R L_R I_R + 8V_R^2)} \tag{23}$$

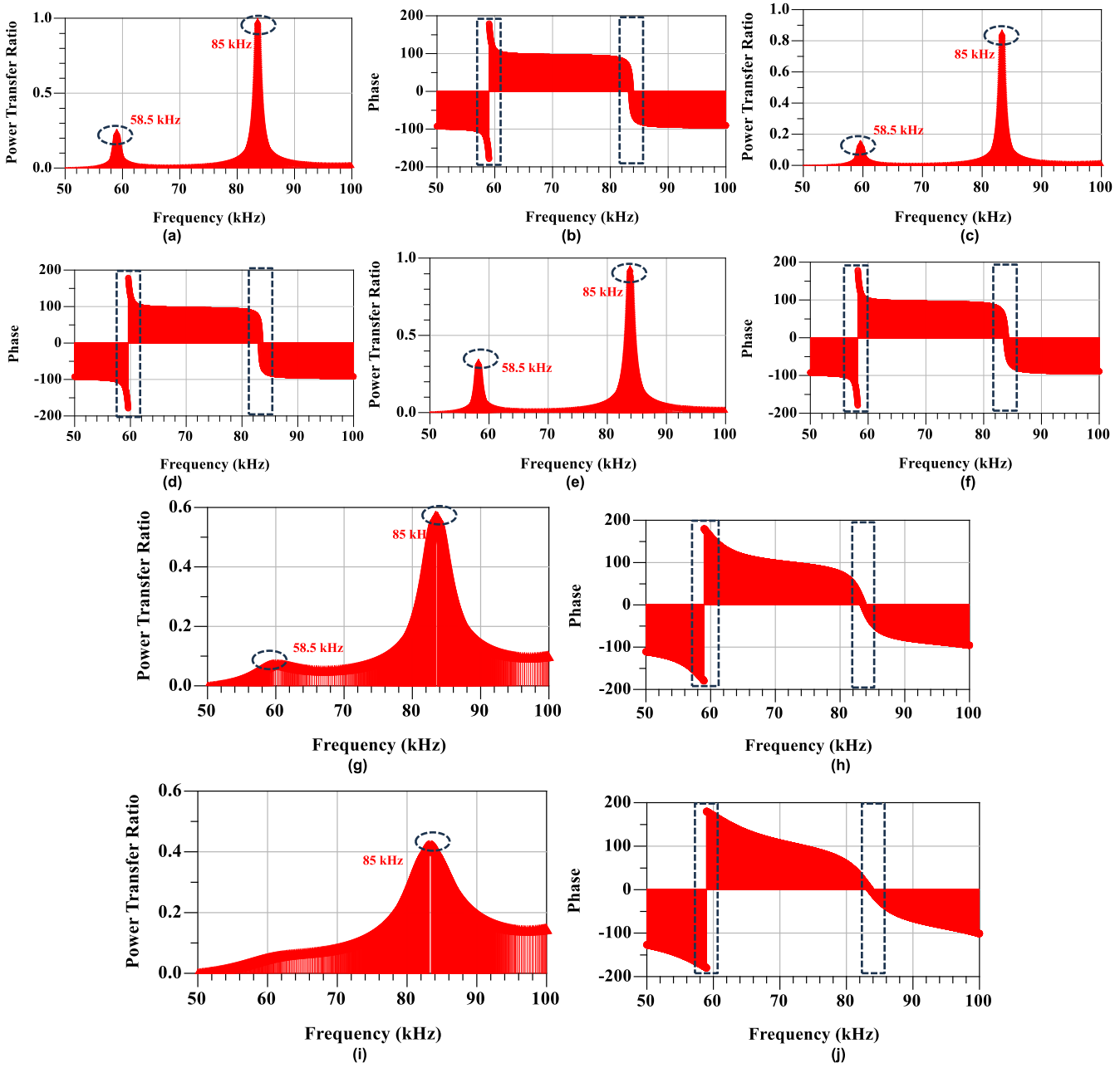

FIGURE 5. CC mode of operation (a) Power transfer ratio at k = 0.25 and R_L = 0.5 Ω (b) Phase plot at k = 0.25 and R_L = 0.5 Ω (c) Power transfer ratio at k = 0.15 and R_L = 0.5 Ω (d) Phase plot at k = 0.15 and R_L = 0.5 Ω (e) Power transfer ratio at k = 0.35 and R_L = 0.5 Ω (f) Phase plot at k = 0.35 and R_L = 0.5 Ω (g) Power transfer ratio at k = 0.25 and R_L = 5 Ω (h) Phase plot at k = 0.25 and R_L = 5 Ω (i) Power transfer ratio at k = 0.25 and R_L = 5 Ω (j) Phase plot at k = 0.25 and R_L = 10 Ω.

The simulation analysis of the frequency sweep characteristics of the S-LCC network under the CC and CV mode of operation are plotted in Figure 5 and Figure 6. Figure 5 shows a frequency sweep for different load resistances (R_L) and coupling coefficients (k) to show the response curve of the total input impedance. The magnitude plot of the total impedances is shown in Figures 6(a)–(b) and (e)–(f), while the phase plot is shown in Figures 6(c)–(d) and (g)–(h). The coupling coefficient (k) of the system, with the calculated critical value of 0.247, must be less than k_c in order to assure optimal performance. R_L, or load resistance, changes depending on the coupling. The following observations are made from the analysis.

- The coupling coefficient needs to be maintained slightly lower than the critical value to avoid the bifurcation effect.
- The high Q coil internal resistance values are minimum as compared to the load resistance value.

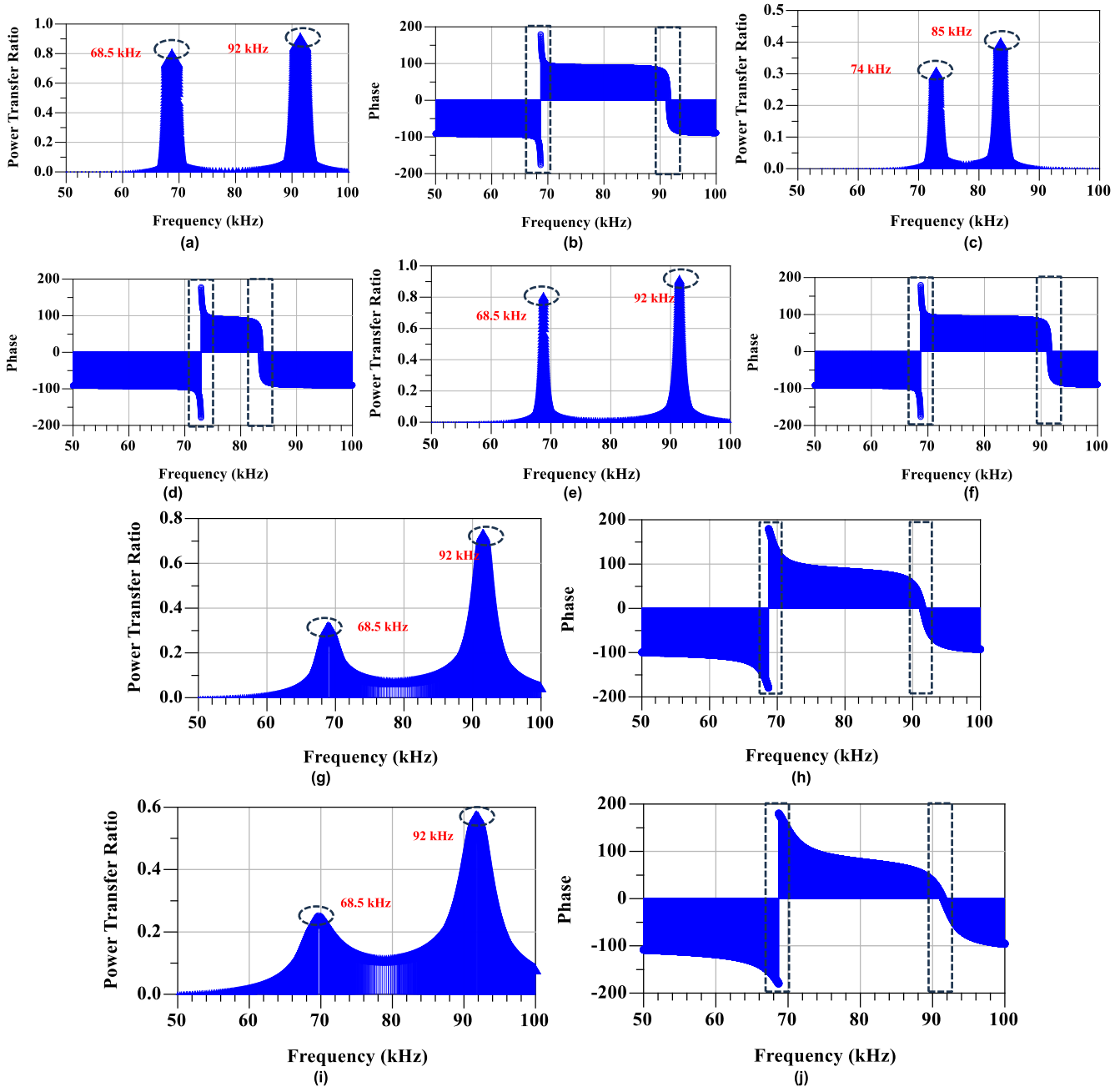

FIGURE 6. CV mode of operation (a) Power transfer ratio at k = 0.25 and R_L = 0.5 Ω (b) Phase plot at k = 0.25 and R_L = 0.5 Ω (c) Power transfer ratio at k = 0.15 and R_L = 0.5 Ω (d) Phase plot at k = 0.15 and R_L = 0.5 Ω (e) Power transfer ratio at k = 0.35 and R_L = 0.5 Ω (f) Phase plot at k = 0.35 and R_L = 0.5 Ω (g) Power transfer ratio at k = 0.25 and R_L = 5 Ω (h) Phase plot at k = 0.25 and R_L = 5 Ω (i) Power transfer ratio at k = 0.25 and R_L = 5 Ω (j) Phase plot at k = 0.25 and R_L = 10 Ω.

- The ON state resistance loss of the switches are minimum
- The impact of the load variation with the CC and CV mode of operation are balanced using hybrid compensators.

At two distinct frequencies, the impedance curve and power transfer ratio splits, and the system's concerned voltage gain achieves its maximum. For various load and coupling modifications, the two separate bifurcation frequencies are obtained. At the resonant frequency, the phase angle is zero. According to SAE, the charging system's operating resonance frequency is 85 kHz. At the resonance frequency for the problematic k variations, the |zin| is lowest. The phase plot is distinct from other k values when k hits a minimum value, such as k = 0.1, where there is only one minimal |Zin|. To achieve the soft switching, the phase angle must always be positive and marginally larger than the resonant frequency.

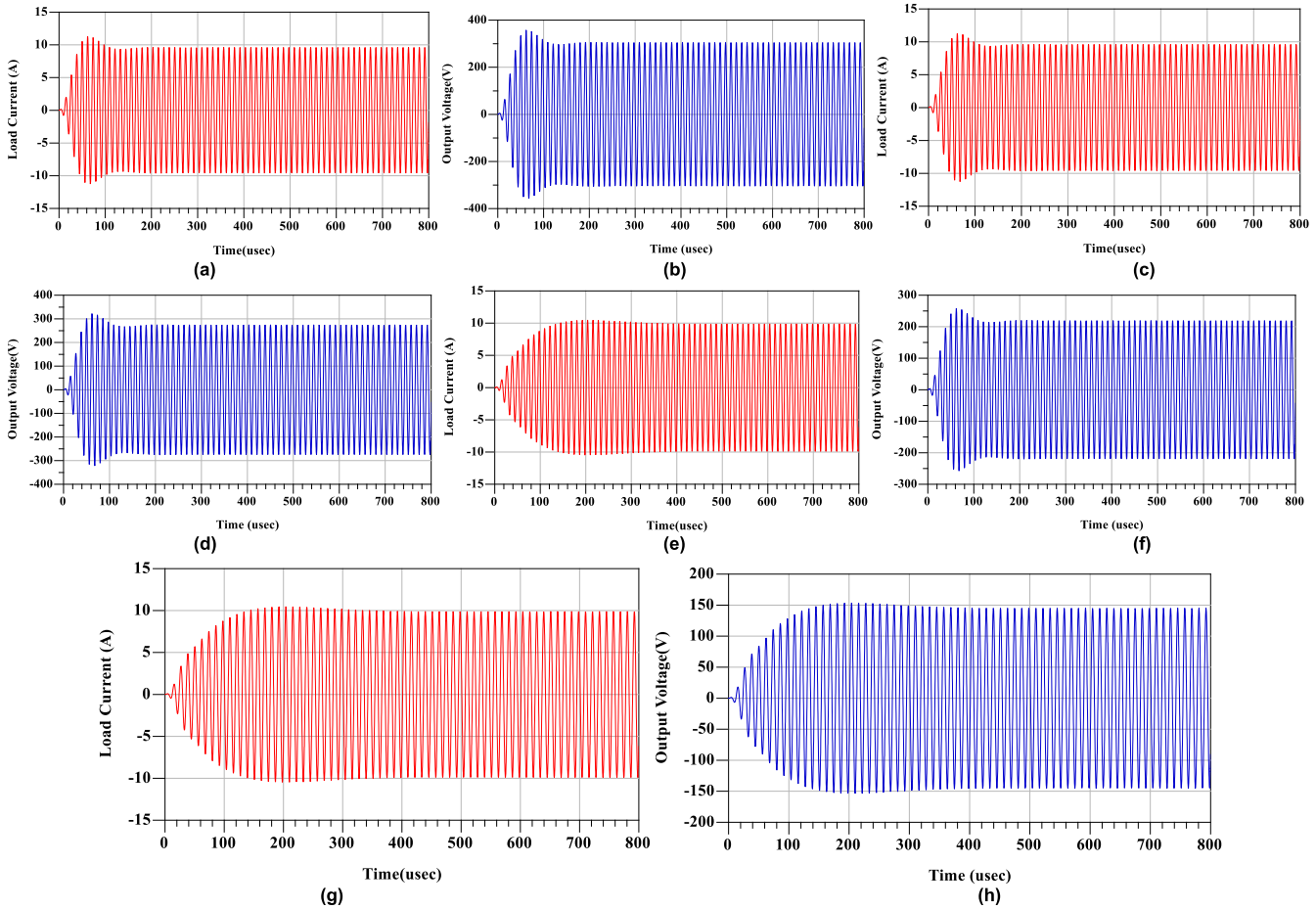

FIGURE 7. CC mode of operation measured load voltage and current (a) I_L at 100% R_L (b) V_L at 100% R_L (c) I_L at 75% R_L (d) V_L at 75% R_L (e) I_L at 50% R_L (f) V_L at 50% R_L (g) I_L at 25% R_L (h) V_L at 25% R_L.

D. SIMULATION RESPONSE ANALYSIS

The developed circuit is modelled for the mentioned power rating of 3.3 kW and 85 kHz operating frequency. The load voltage and load current at different load resistance conditions are measured namely 25%, 50%, 75%, 100% of load resistance to validate the CC mode of operation. Similarly, to validate the CV mode the measured resistance are 125%, 150%, 175% and 200%. From the following analysis results it is observed that the load voltage is rising during the CC mode of operation maintaining the load current as constant value of 8.85 A. On the other side, the CV mode of operation maintains the load voltage as constant at 350 V with decrease in the load current value. Figure 7 and Figure 8 illustrate the measured load voltage and current waveform at different load resistance values. The receiver side measurements are performed after the compensators, which will be further converted to the DC voltage by a rectifier. The measured voltage and current response indicate that the proposed hybrid compensation is effective for the different SOC levels of the battery with simple auxiliary switch to turn from CC to CV mode of operation. During the CC mode of operation, the voltage across the load side increasing as the equivalent resistance value is increased towards the rated resistance value. Figure 7(b), (d) and (f) indicate that the corresponding changes in the load voltage by maintaining the load current as constant. On the other side, during the CV mode of operation, the load current rises when the load resistance value is reduced from the rated value. Moreover, the load voltage is kept constant irrespective of the changes in the equivalent resistance value. Figure 8(a), (c), (e), (g) indicates the corresponding changes in the load current in CV mode of operation.

E. CHARGING COUPLERS

The wireless charging system hinges on the prowess of its charging couplers an indispensable element that governs the efficiency, security, and reliability of the entire charging process. When delving into the selection process for an appropriate charging coupler, a multifaceted approach is imperative to address key considerations. These encompass the coupler's resilience against misalignment, its interoperability with various devices, its capacity for efficient heat dissipation, the optimal power transmission distance, and the overall efficacy of the charging system. In the context of this project, the DD

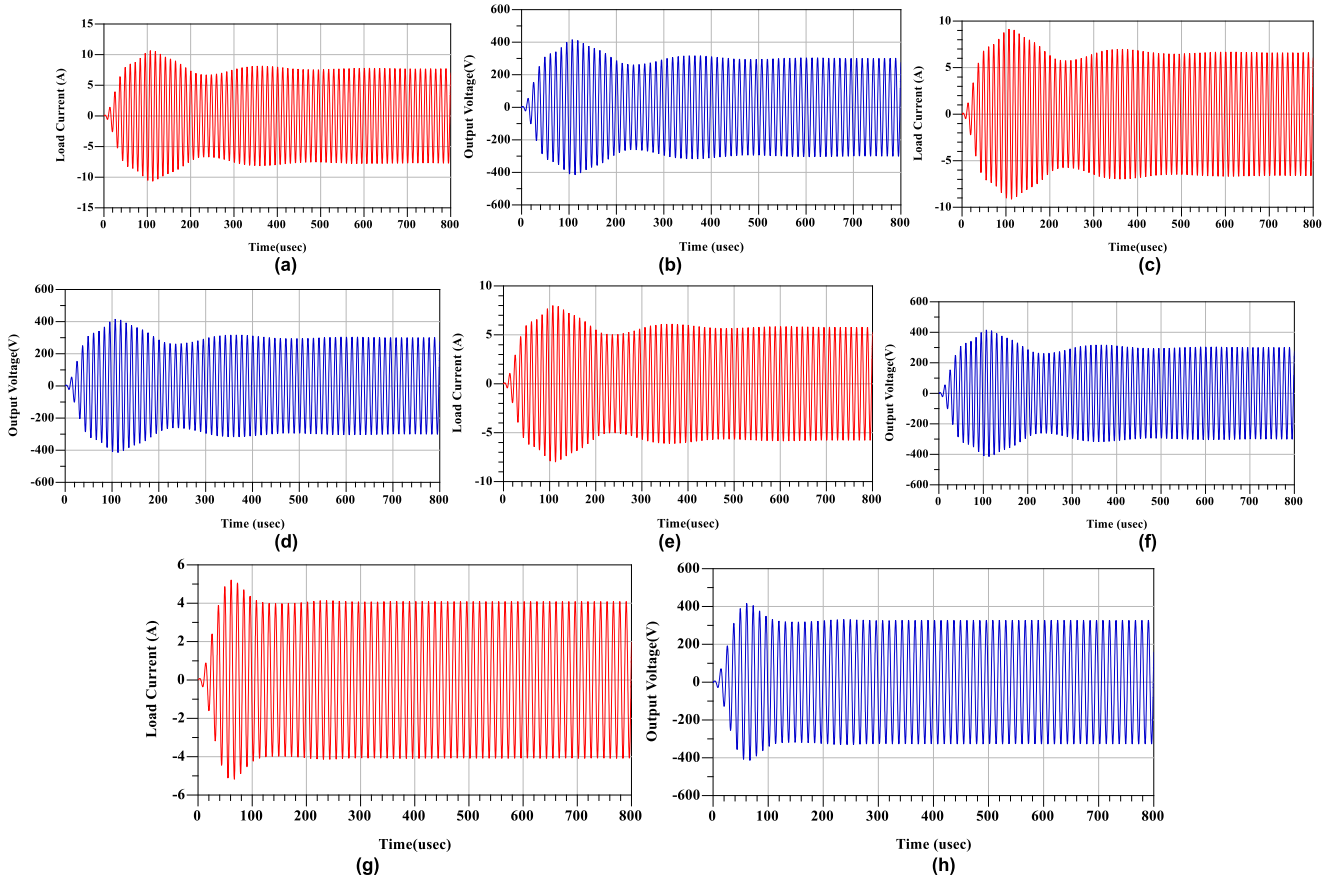

FIGURE 8. CV mode of operation measured load voltage and current (a) I_L at 125% R_L (b) V_L at 125% R_L (c) I_L at 150% R_L (d) V_L at 150% R_L (e) I_L at 175% R_L (f) V_L at 175% R_L (g) I_L at 200% R_L (h) V_L at 200% R_L.

coupler emerged as the prime choice owing to its remarkable tolerance to horizontal misalignment. This attribute plays a pivotal role in enhancing the robustness of the wireless charging system, ensuring that even in scenarios where alignment may not be perfect, the charging process remains unaffected. Figure 9 serves as a comprehensive visual aid, elucidating the intricate configuration and precise dimensions of the selected charging coupler.

To delve further into the technical intricacies, the utilization of the eddy current solver within the ANSYS Finite Element Analysis (FEA) program stands out as a crucial aspect of the design process. This solver is instrumental in deriving the required inductance with predefined dimensions. The in-depth simulations facilitated by ANSYS FEA enable engineers to make nuanced adjustments, such as modifications to the specified American Wire Gauge (AWG) and alterations in the number of strands. In essence, the ANSYS FEA program provides a virtual testing ground where engineers can iteratively refine the charging coupler design. This iterative process allows for the optimization of critical parameters, ensuring that the coupler aligns seamlessly with the project's specifications. The ability to fine-tune parameters like AWG and strand count empowers designers to tailor the charging coupler to meet the exacting demands of the wireless

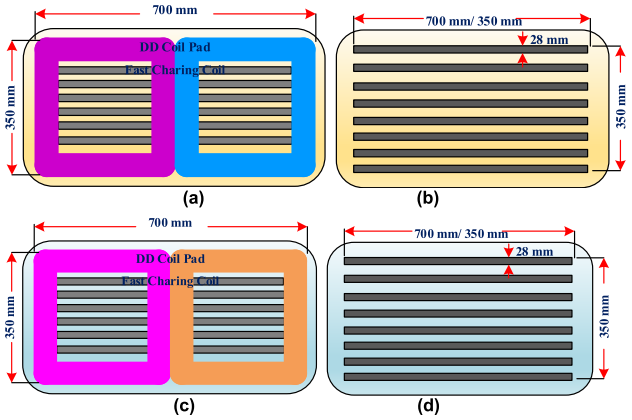

FIGURE 9. DD charging couplers arrangement (a) Transmitter pad (b) Ferrite arrangements (c) Receiver pad (d) Ferrite arrangements.

charging system. In the pursuit of attaining the desired outcomes, a meticulous approach is taken in configuring the wireless charging system. The strategic alignment of both the operating resonant frequency and excitation current at 85 kHz lays the foundation for optimal performance. Leveraging stochastic variations in the number of turns and ferrites

TABLE 1. DD pad parameters.

Parameters	Values
Number of Strands	1050
AWG	38
Size of the Transmitter Pad	700 mm X350 mm
Transmitter Pad Inductance, L_T	229 µH
Size of the Receiver Pad	700 mm X350 mm
Receiver Pad Inductance, L_R	225.4 µH
Ferrite Dimension	55*45*9 mm
Mutual Inductance, L_M	56.34 µH
Aluminium Shielding Thickness	2 mm

introduces a nuanced tool that facilitates the determination of crucial parameters such as the ideal inner distance, gap between turns, and the number of turns. The inductance of the charging pad is a pivotal aspect influenced by multiple factors, including the charging coil, ferrite core structure, and aluminum shielding. The utilization of the CF297 family of cosmo ferrite bars underscores a deliberate choice in material, adding a layer of precision to the charging pad's inductance characteristics. This selection is pivotal in ensuring that the charging pad resonates harmoniously with the rest of the system.

Moving to the charging coupler, its mutual inductance is a dynamic parameter influenced by a trifecta of factors—current gain (Ig), load resistance (RL), and resonant frequency (fr). The calculated load resistance, tailored to supply 350 V and 3300 W, becomes a crucial determinant in shaping the performance characteristics. The interplay between rated power, delivery voltage, and current gain adds a layer of complexity that demands a nuanced approach to optimization. The receiver pad coil inductance (LR) is intricately linked to the product of Q and RL, with an inverse relationship to fr when assuming Q to be 5 and fr to be 85 kHz. This mathematical interdependence underscores the importance of precision in tuning these parameters to achieve the desired inductance profile. The use of 3D printers in crafting ferrite core slots and coil trays showcases a commitment to precision manufacturing, allowing for the creation of intricate components with the utmost accuracy. The establishment of an ideal distance of 1 mm between each coil turn is a testament to the attention to detail in the design process. This meticulous spacing is pivotal when the receiver pad is positioned over the transmitter pad, ensuring that power transfer occurs seamlessly without compromising the power transfer profile and trans-coupling inductance. Presenting the charging coupler parameters in Table 1 provides a comprehensive snapshot of the system's specifications, aiding in clarity and facilitating further analysis. The magnetic field spectrum, derived through the Finite Element Analysis (FEA) tool, is visually represented in Figure 8. This spectrum becomes a valuable reference, particularly when the receiver pad undergoes horizontal movement, revealing fluctuations in mutual inductance based on the alignment with the transmitter pad. Figure 10 serves as a visual guide, enabling engineers to assess the system's performance dynamically and make informed adjustments for optimal wireless charging efficiency.

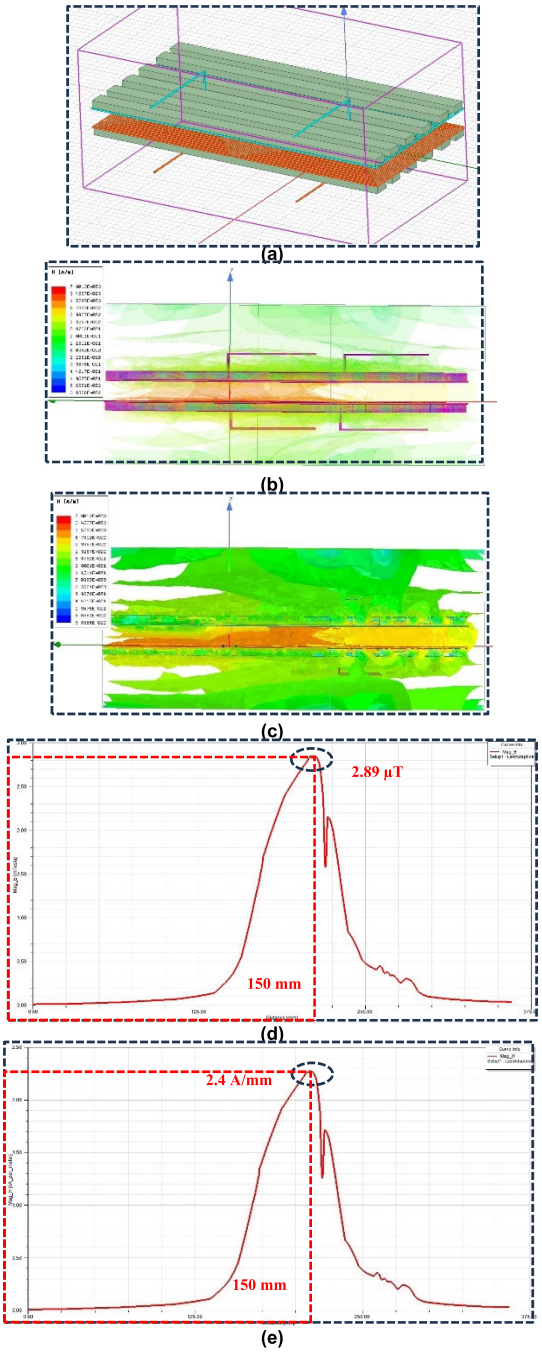

FIGURE 10. Magnetic flux distribution (a) DD coil design with ferrites (b) Front view of field distribution (c) Field distribution pattern (d) Magnetic flux density variation under air gap variation (e) Magnetic field intensity variation under air gap variation.

III. EXPERIMENTAL ANALYSIS

In the exploration of advanced energy systems, a notable innovation takes center stage a 3.3 kW PV-integrated hybrid

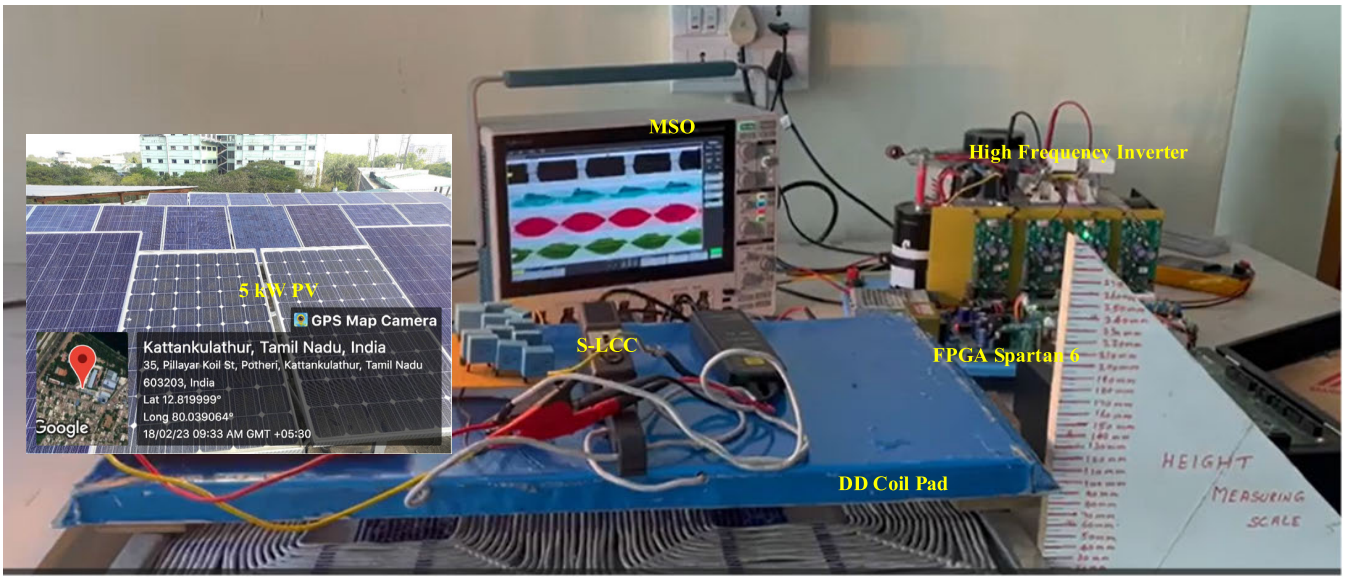

FIGURE 11. Experimental setup of the proposed PV integrated WPT system.

TABLE 2. Comparison of the proposed approach with other literature.

Ref.	Compensation Topology	PV Integration Investigated	Power Rating	Operating Frequency	CC/CV Mode	Z Gap (mm)	Efficiency (%)	Remarks
[58]	Series – Series	Yes	100 W	85 kHz	NO	150	83%	The SS- compensated WPT system investigated with PV integration.
[59]	LCC-S	No	1 kW	85 kHz	Yes	100	87%	The simulation analysis is performed for the limited gap between the pad with output voltage regulation.
[60]	S-LCC	No	200 W	100 kHz	NO	100	NM	S-LCC topology proposed for the Electric Bicycles to optimize the number of passive components.
[61]	LCC-LCC	No	400 W	140 kHz	Yes	120	91.2	ADRC controller is designed to regulate the output voltage. Requires communication to make it as closed loop control.
[62]	LCL-S	No	1.3 kW	85 kHz	Yes	200	90.5	Modular design of LCL proposed to overcome the misalignment challenges.
Proposed	S-SP/LCC	Yes	3.3 kW	85 kHz	Yes	150	91.3	The PV system is integrated with the hybrid compensated WPT system to provide the CC/CV mode of operation without receiver side communications.

compensated constant wireless charging system. A 5 kW solar panel array, seamlessly integrated into the system's architecture as shown in Figure 11. Through the implementation of a boost converter, these solar panels contribute DC power to the DC bus, forming a pivotal link in the energy generation chain. This design not only harnesses the abundant solar power during peak generation but also incorporates an ingenious energy storage device. This device acts as a reliable reservoir, stepping in to supply the required charging power during periods when solar energy availability falls short. The functionality of the inverter is a key highlight, leveraging Silicon Carbide (SiC) based Metal-Oxide-Semiconductor Field-Effect Transistors (MOSFETs) to efficiently handle the constant DC input from the DC bus. Driving signals for the MOSFETs are programmed with precision by the FPGA SPARTAN controller. The compensating circuits within the system exhibit a commitment to quality, employing KEMET capacitors and ferrite-cored inductors. This deliberate choice of components reflects a dedication to ensuring optimal performance and stability within the wireless charging system. The utilization of SiC components in the rectifier diodes and auxiliary switch underscores a forward-thinking approach,

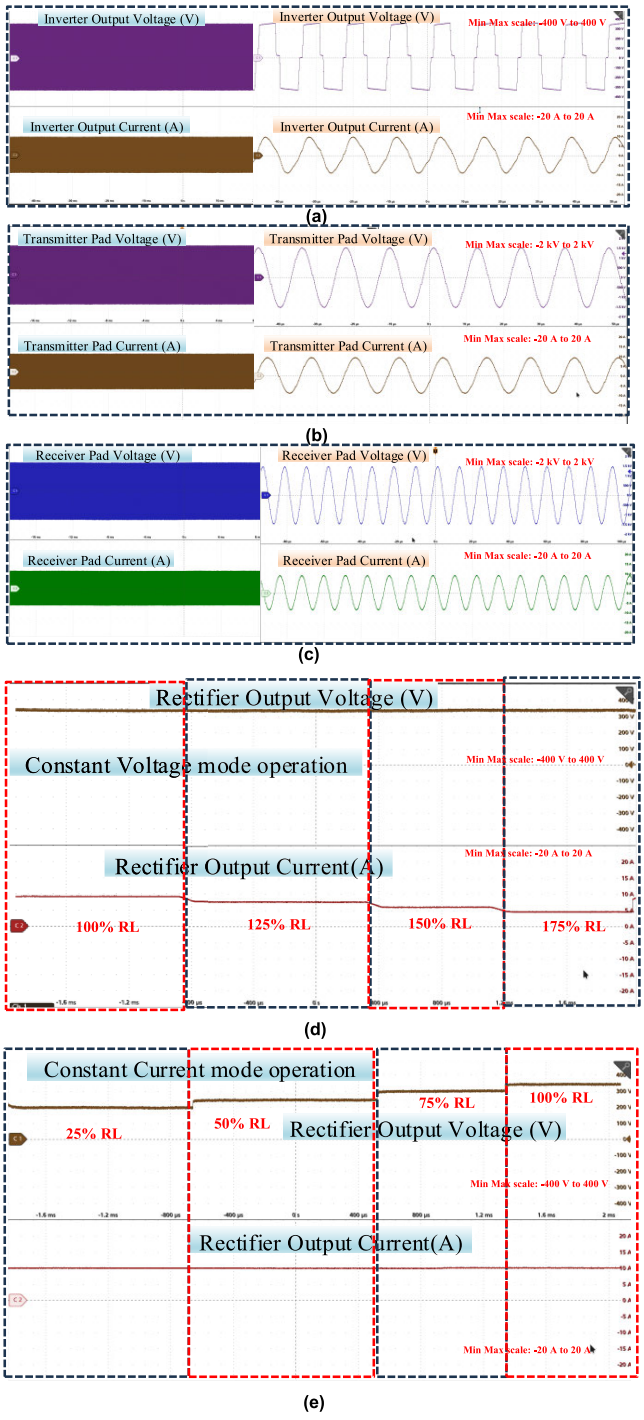

FIGURE 12. Experimental waveforms (a) Inverter output voltage and current (b) Transmitter pad voltage and current (c) Receiver pad voltage and current (d) Constant voltage mode of operation (e) Constant current mode of operation.

capitalizing on the superior characteristics of Silicon Carbide in terms of efficiency and reliability. As the battery voltage approaches its rated value, the system responds dynamically, sending driving pulses to the auxiliary switches.

This adaptive mechanism enhances the precision of the charging process, ensuring the battery is charged with utmost efficiency and safety. Under load resistance circumstances, the charging system impressively generates 350 V and 8.85 A, further attesting to its capability in delivering reliable and high-performance wireless charging. The charging system keeps the current flowing steadily until the EV battery voltage exceeds the predetermined level. The receiver-side controller receives data from the voltage sensor, which detects the battery voltage. The controller then transmits driving signals to turn on and off the auxiliary switch. This switch functions in parallel with the receiver-side compensating inductor, and when it is in the ''on'' position, its anti-parallel counterpart conducts. The auxiliary switch is turned off during this time, and the receiver-side compensating inductor maintains a steady current flow to the EV's battery. The receiver-side resonant network in this mode is designed as an LCC network. To replicate the continuous current mode, the loading resistance is changed at intervals of 25%, 50%, 75%, and 100% of its rated value. Despite variations in the load, the current provided to the battery stays constant. Under rated load conditions, the voltage gradually increases until it reaches the rated amount. The experimental waveforms for the S-LCC network and CC mode are shown in Figure 12. The voltage and current waveforms of the inverter, transmitter and receiver pads, high-frequency rectifier, and boost converter are shown in Figures 12(a)–(e). The voltage and current in the CC mode inverter are shown in Figure 12(e). The receiver-side controller sends high driving pulses to the auxiliary switch once the battery reaches its rated voltage. Once the battery exceeds the rated voltage, the charging system maintains a constant voltage. The controller instructs the auxiliary switch to disconnect the compensation inductor when it detects the battery voltage. The current flow via the switch is then started when the auxiliary switch is activated. Driving pulses are sent to the auxiliary switch via the receiver side controller, which enables full battery charge. The receiver-side compensating inductor is disconnected from the network, resulting in an SP topology for the resonant network. A constant voltage supply to the charging device is made possible by the parallel capacitor. The experimental waveforms for the S-SP structure are shown in Figure 12(d). To obtain the CV mode response curve, the load resistance is increased by 100%, 125%, 150%, and 175%. In this mode, the system maintains a constant voltage while supplying less current. The auxiliary switch is then turned off and the charging mechanism remains in this mode until the battery reaches a complete 100% charge. It is interesting that in both modes, the operating resonant frequency does not change.

The loss presents during the CC, CV mode at different rated load conditions is present in the network are primarily at the coupler side, high frequency inverter, rectifier, and compensator units. The variation in the power loss is due to changes in the rated load condition, coupling coefficient. As the transition from CC to CV mode occurs with rated load condition, the losses present in the coupler is reduces. On the other side the whenever, the load is not equal to the rated value

the power losses are predominantly present over the coupler and compensating unit.

IV. CONCLUSION

This paper introduces a PV integrated hybrid compensated WPT system that drives a receiver-side tuned resonant network-equipped constant wireless charging system. In addition to series compensation on the transmitter side, the control mechanism on the receiver side guarantees a consistent charging experience with constant current and voltage. The auxiliary switch facilitates mode changes, which are directed by driving pulses from the receiver-side controller in response to changes in battery voltage. Notably, this control method does away with the requirement for ground-to-vehicle communication. The MPPT dc-dc converter keeps the voltage at the dc bus constant while the charging system is powered by the PV source and an energy storage device. Importantly, the proposed charging system runs independently of the utility grid, preventing it from adding to the network's growing power consumption. Due to its constant D.C. bus fed design, the stand-alone PV system consumes less power than a grid-connected system when charging the EV battery during periods of high irradiation. Even though the standalone PV integrated charging system primarily uses solar electricity, future utility grid interconnection is anticipated. The capacity to feed extra energy back into the grid during the generation of surplus electricity in high irradiation circumstances increases the system's adaptability and promotes grid sustainability. The limitation associated with the proposed system is that the absence of PV will make the system depend on the Grid or energy storage unit. However, the proposed system will cumulatively increase the usage of PV. Another limitation is that the pre calculation and design need to be done for the hybrid compensators considering the load and coupling variation to avoid the frequency bifurcation.

ACKNOWLEDGMENT

The authors acknowledge the Researchers Supporting Project, King Saud University, Riyadh, Saudi Arabia, under Grant RSP2024R467; and also the Government of India, Department of Science and Technology (DST) Science and Engineering Research Board (SERB) Core Re-Search under Grant CRG/2020/004073.

REFERENCES

[1] J. Gao, Z. Wang, X. Li, and X. Zhou, "Investigation of a novel scheme utilizing solar and geothermal energies, generating power and ammonia: Exergoeconomic and exergoenvironmental analyses and cuckoo search optimization," *Energy*, vol. 298, Jul. 2024, Art. no. 131I344, doi: 10.1016/j.energy.2024.131344.

[2] Z. Ma, J. Zhao, L. Yu, M. Yan, L. Liang, X. Wu, M. Xu, W. Wang, and S. Yan, "A review of energy supply for biomachine hybrid robots," *Cyborg Bionic Syst.*, vol. 4, p. 53, Jan. 2023, doi: 10.34133/cbsystems.0053.

[3] C. Yang, T. U. Kumar Nutakki, M. A. Alghassab, S. Alkhalaf, F. Alturise, F. S. Alharbi, Y. Elmasry, and S. Abdullaev, "Optimized integration of solar energy and liquefied natural gas regasification for sustainable urban development: Dynamic modeling, data-driven optimization, and case study," *J. Cleaner Prod.*, vol. 447, Apr. 2024, Art. no. 141405, doi: 10.1016/j.jclepro.2024.141405.

[4] J. Fan and X. Zhou, "Optimization of a hybrid solar/wind/storage system with bio-generator for a household by emerging metaheuristic optimization algorithm," *J. Energy Storage*, vol. 73, Dec. 2023, Art. no. 108967, doi: 10.1016/j.est.2023.108967.

[5] X. Zhang, Y. Wang, X. Yuan, Y. Shen, Z. Lu, and Z. Wang, "Adaptive dynamic surface control with disturbance observers for battery/supercapacitor-based hybrid energy sources in electric vehicles," *IEEE Trans. Transport. Electrific.*, vol. 9, no. 4, pp. 5165–5181, Apr. 2022, doi: 10.1109/TTE.2022.3194034.

[6] X. Zhang, Z. Lu, X. Yuan, Y. Wang, and X. Shen, "L2-gain adaptive robust control for hybrid energy storage system in electric vehicles," *IEEE Trans. Power Electron.*, vol. 36, no. 6, pp. 7319–7332, Jun. 2021, doi: 10.1109/TPEL.2020.3041653.

[7] X. Zhang, Z. Wang, and Z. Lu, "Multi-objective load dispatch for microgrid with electric vehicles using modified gravitational search and particle swarm optimization algorithm," *Appl. Energy*, vol. 306, Jan. 2022, Art. no. 118018, doi: 10.1016/j.apenergy.2021.118018.

[8] *The Global Electric Vehicle Market In 2023*. Accessed: May 22, 2023. [Online]. Available: https://www.virta.global/en/global-electric-vehicle-market

[9] Niti Aayog. *E-Amrit Charging Infrastructure*. Accessed: Sep. 25, 2023. [Online]. Available: https://e-amrit.niti.gov.in/infrastructure

[10] J. Liang, J. Feng, Z. Fang, Y. Lu, G. Yin, X. Mao, J. Wu, and F. Wang, "An energy-oriented torque-vector control framework for distributed drive electric vehicles," *IEEE Trans. Transp. Electrific.*, vol. 9, no. 3, pp. 4014–4031, Mar. 2023, doi: 10.1109/TTE.2022.3231933.

[11] B. Shao, Q. Xiao, L. Xiong, L. Wang, Y. Yang, Z. Chen, F. Blaabjerg, and J. M. Guerrero, "Power coupling analysis and improved decoupling control for the VSC connected to a weak AC grid," *Int. J. Electr. Power Energy Syst.*, vol. 145, Feb. 2023, Art. no. 108645, doi: 10.1016/j.ijepes.2022.108645.

[12] J. Linru, Z. Yuanxing, L. Taoyong, D. Xiaohong, and Z. Jing, "Analysis on charging safety and optimization of electric vehicles," in *Proc. IEEE 6th Int. Conf. Comput. Commun. (ICCC)*, Chengdu, China, Dec. 2020, pp. 2382–2385, doi: 10.1109/ICCC51575.2020.9344906.

[13] X. Diao, L. Jiang, T. Gao, L. Zhang, J. Zhang, L. Wang, and Q. Wu, "Research on electric vehicle charging safety warning based on A-LSTM algorithm," *IEEE Access*, vol. 11, pp. 55081–55093, 2023, doi: 10.1109/ACCESS.2023.3281552.

[14] S. Yuvaraja and R. Narayanamoorthi, "A five leg converter with multi-transmitter for an in-motion charging system," *J. Phys., Conf. Ser.*, vol. 2335, no. 1, Sep. 2022, Art. no. 012054, doi: 10.1088/1742-6596/2335/1/012054.

[15] K. Cao, H. Ding, W. Li, L. Lv, M. Gao, F. Gong, and B. Wang, "On the ergodic secrecy capacity of intelligent reflecting surface aided wireless powered communication systems," *IEEE Wireless Commun. Lett.*, vol. 11, no. 11, pp. 2275–2279, Nov. 2022, doi: 10.1109/LWC.2022.3199593.

[16] Y. Shanmugam, R. Narayanamoorthi, P. Vishnuram, M. Bajaj, K. M. AboRas, P. Thakur, and Kitmo, "A systematic review of dynamic wireless charging system for electric transportation," *IEEE Access*, vol. 10, pp. 133617–133642, 2022.

[17] J. Jose and J. P. Therattil, "WPT compensation topology optimized for PV embedded electric vehicle," *Sustain. Energy Technol. Assessments*, vol. 53, Oct. 2022, Art. no. 102605, doi: 10.1016/j.seta.2022.102605.

[18] N. Mohamed, A. Flah, and B. H. Mouna, "Characteristic of photovoltaic generator for the electric vehicle," *Int. J. Sci. Technol. Res.*, vol. 8, no. 10, pp. 871–876, 2019.

[19] S. A. Mirbozorgi, H. Bahrami, M. Sawan, and B. Gosselin, "A smart multicoil inductively coupled array for wireless power transmission," *IEEE Trans. Ind. Electron.*, vol. 61, no. 11, pp. 6061–6070, Nov. 2014, doi: 10.1109/TIE.2014.2308138.

[20] S. Pahlavan and S. J. Ashtiani, "Rotation-tolerant wireless power transmission scheme with smart positioning for cognitive research on moving animals," *IEEE Trans. Biomed. Circuits Syst.*, vol. 18, no. 1, pp. 123–130, Feb. 2024, doi: 10.1109/TBCAS.2023.3314913.

[21] S. Pahlavan, M. Shooshtari, and S. J. Ashtiani, "Star-shaped coils in the transmitter array for receiver rotation tolerance in free-moving wireless power transfer applications," *Energies*, vol. 15, no. 22, p. 8643, Nov. 2022, doi: 10.3390/en15228643.

[22] N. Ri, "Cross interference free dual frequency wireless power transfer using frequency bifurcation for dynamic biomedical implants," *IEEE Trans. Electromagn. Compat.*, vol. 63, no. 1, pp. 286–293, Feb. 2021, doi: 10.1109/TEMC.2020.2984517.

[23] S. Yuvaraja, R. Narayanamoorthi, J. S. M. Ali, and D. Almakhles, "A comprehensive review of the on-road wireless charging system for E-mobility applications," *Frontiers Energy Res.*, vol. 10, Jul. 2022, doi: 10.3389/fenrg.2022.926270.

[24] J. Rahulkumar, R. Narayanamoorthi, P. Vishnuram, C. Balaji, T. Gono, T. Dockal, R. Gono, and P. Krejci, "A review on resonant inductive coupling pad design for wireless electric vehicle charging application," *Energy Rep.*, vol. 10, pp. 2047–2079, Nov. 2023, doi: 10.1016/j.egyr.2023.08.067.

[25] J. Rahulkumar, R. Narayanamoorthi, P. Vishnuram, M. Bajaj, V. Blazek, L. Prokop, and S. Misak, "An empirical survey on wireless inductive power pad and resonant magnetic field coupling for in-motion EV charging system," *IEEE Access*, vol. 11, pp. 4660–4693, 2023.

[26] V. Ramakrishnan, A. D. Savio, C. Balaji, N. Rajamanickam, H. Kotb, A. Elrashidi, and W. Nureldeen, "A comprehensive review on efficiency enhancement of wireless charging system for the electric vehicles applications," *IEEE Access*, vol. 12, pp. 46967–46994, 2024, doi: 10.1109/ACCESS.2024.3378303.

[27] L. Lu, W. Wu, Y. Gao, C. Pan, X. Yu, C. Zhang, and Z. Jin, "Study on current discrepancy and redistribution of HTS non-insulation closed-loop coils during charging/discharging and subsequent transient process toward steady-state operation," *Superconductor Sci. Technol.*, vol. 35, no. 9, Sep. 2022, Art. no. 095001, doi: 10.1088/1361-6668/ac7dfe.

[28] Y. Shanmugam, R. Narayanamoorthi, P. Vishnuram, D. Savio, A. Yadav, M. Bajaj, A. Nauman, T. Khurshaid, and S. Kamel, "Solar-powered five-leg inverter-driven quasi-dynamic charging for a slow-moving vehicle," *Frontiers Energy Res.*, vol. 11, pp. 1–16, Mar. 2023, doi: 10.3389/fenrg.2023.1115262.

[29] W.-T. Lee, M.-L. Kung, and K.-H. Lin, "P-impedance matching circuit for wireless power transfer systems under dynamic load and transfer distance," in *Proc. IEEE Int. Symp. Antennas Propag. North Amer. Radio Sci. Meeting*, Montreal, QC, Canada, Jul. 2020, pp. 1579–1580, doi: 10.1109/IEEECONF35879.2020.9330190.

[30] M. Venkatesan, R. Narayanamoorthi, K. M. AboRas, and A. Emara, "Efficient bidirectional wireless power transfer system control using dual phase shift PWM technique for electric vehicle applications," *IEEE Access*, vol. 12, pp. 27739–27755, 2024, doi: 10.1109/ACCESS.2024.3367437.

[31] X. Huang and L. He, "Stable and efficient class E2 wireless power transfer system based on parity-time symmetry," in *Proc. IEEE PELS Workshop Emerg. Technologies: Wireless Power Transf. (WoW)*, San Diego, CA, USA, Jun. 2021, pp. 1–4, doi: 10.1109/WoW51332.2021.9462866.

[32] Z. Fang, J. Wang, J. Liang, Y. Yan, D. Pi, H. Zhang, and G. Yin, "Authority allocation strategy for shared steering control considering human–machine mutual trust level," *IEEE Trans. Intell. Vehicles*, vol. 9, no. 1, pp. 2002–2015, Jan. 2024, doi: 10.1109/TIV.2023.3300152.

[33] X. Xu, W. Liu, and L. Yu, "Trajectory prediction for heterogeneous traffic-agents using knowledge correction data-driven model," *Inf. Sci.*, vol. 608, pp. 375–391, Aug. 2022, doi: 10.1016/j.ins.2022.06.073.

[34] W. Gu, D. Qiu, X. Shu, B. Zhang, W. Xiao, and Y. Chen, "A constant output capacitive wireless power transfer system based on parity-time symmetric," *IEEE Trans. Circuits Syst. II, Exp. Briefs*, vol. 70, no. 7, pp. 2585–2589, Jul. 2023, doi: 10.1109/TCSII.2023.3237687.

[35] L. Zhao, H. Xu, S. Qu, Z. Wei, and Y. Liu, "Joint trajectory and communication design for UAV-assisted symbiotic radio networks," *IEEE Trans. Veh. Technol.*, vol. 73, no. 6, pp. 8367–8378, Jun. 2024, doi: 10.1109/TVT.2024.3356587.

[36] C. Wang, Y. Wang, K. Wang, Y. Dong, and Y. Yang, "An improved hybrid algorithm based on biogeography/complex and metropolis for many-objective optimization," *Math. Problems Eng.*, vol. 2017, no. 1, 2017, Art. no. 2462891, doi: 10.1155/2017/2462891.

[37] R. Wang, Q. Gu, S. Lu, J. Tian, Z. Yin, L. Yin, and W. Zheng, "FI-NPI: Exploring optimal control in parallel platform systems," *Electronics*, vol. 13, no. 7, p. 1168, Mar. 2024, doi: 10.3390/electronics13071168.

[38] J. Chen, J. Xu, Y. Zhang, J. Zhao, J. Hou, and Y. Wang, "Geometrical state-plane-based synchronous rectification scheme for LLC converter in EVs," *IEEE Trans. Transport. Electrific.*, early access, 2024, doi: 10.1109/TTE.2024.3383208.

[39] J. Zhou, B. Zhang, W. Xiao, D. Qiu, and Y. Chen, "Nonlinear parity-time-symmetric model for constant efficiency wireless power transfer: Application to a drone-in-flight wireless charging platform," *IEEE Trans. Ind. Electron.*, vol. 66, no. 5, pp. 4097–4107, May 2019, doi: 10.1109/TIE.2018.2864515.

[40] X. Bai, M. Xu, Q. Li, and L. Yu, "Trajectory-battery integrated design and its application to orbital maneuvers with electric pump-fed engines," *Adv. Space Res.*, vol. 70, no. 3, pp. 825–841, Aug. 2022, doi: 10.1016/j.asr.2022.05.014.

[41] X. Gao, C. Liu, H. Zhou, W. Hu, Y. Huang, Y. Xiao, Z. Lei, and J. Chen, "Design and analysis of a new hybrid wireless power transfer system with a space-saving coupler structure," *IEEE Trans. Power Electron.*, vol. 36, no. 5, pp. 5069–5081, May 2021, doi: 10.1109/TPEL.2020.3027473.

[42] J. Deng, W. Li, T. D. Nguyen, S. Li, and C. C. Mi, "Compact and efficient bipolar coupler for wireless power chargers: Design and analysis," *IEEE Trans. Power Electron.*, vol. 30, no. 11, pp. 6130–6140, Nov. 2015, doi: 10.1109/TPEL.2015.2417115.

[43] B. Luo, T. Long, L. Guo, R. Dai, R. Mai, and Z. He, "Analysis and design of inductive and capacitive hybrid wireless power transfer system for railway application," *IEEE Trans. Ind. Appl.*, vol. 56, no. 3, pp. 3034–3042, May 2020, doi: 10.1109/TIA.2020.2979110.

[44] X. Qing, Z. Li, X. Wu, Z. Liu, L. Zhao, and Y. Su, "A hybrid wireless power transfer system with constant and enhanced current output against load variation and coupling misalignment," *IEEE Trans. Power Electron.*, vol. 38, no. 10, pp. 13219–13230, Oct. 2023, doi: 10.1109/TPEL.2023.3296274.

[45] J. Song, A. Mingotti, J. Zhang, L. Peretto, and H. Wen, "Fast iterative-interpolated DFT phasor estimator considering out-of-band interference," *IEEE Trans. Instrum. Meas.*, vol. 71, pp. 1–14, 2022, doi: 10.1109/TIM.2022.3203459.

[46] W. Zhang and C. C. Mi, "Compensation topologies of high-power wireless power transfer systems," *IEEE Trans. Veh. Technol.*, vol. 65, no. 6, pp. 4768–4778, Jun. 2016, doi: 10.1109/TVT.2015.2454292.

[47] N. Rasekh, J. Kavianpour, and M. Mirsalim, "A novel integration method for a bipolar receiver pad using LCC compensation topology for wireless power transfer," *IEEE Trans. Veh. Technol.*, vol. 67, no. 8, pp. 7419–7428, Aug. 2018, doi: 10.1109/TVT.2018.2837348.

[48] Z. Dai and J. Wang, "A dual-frequency WPT based on multilayer self-decoupled compact coil and dual CLCL hybrid compensation topology," *IEEE Trans. Power Electron.*, vol. 37, no. 11, pp. 13955–13965, Nov. 2022, doi: 10.1109/TPEL.2022.3183861.

[49] C. K. Hridya, R. H. Kumar, and N. Mayadevi, "Wireless bidirectional power transfer with maximum efficiency point tracking control in electric vehicles," in *Proc. IEEE Int. Conf. Power Electron., Smart Grid Renew. Energy (PESGRE)*, Jan. 2020, pp. 1–7, doi: 10.1109/PESGRE45664.2020.9070704.

[50] G. RamChandra Mouli, P. Vanduijsen, T. Velzeboer, G. Nair, Y. Zhao, A. Jamodkar, O. Isabella, S. Silvester, P. Bauer, and M. Zeman, "Solar powered e-bike charging station with AC, DC and contactless charging," in *Proc. 20th Eur. Conf. Power Electron. Appl. (EPE ECCE Europe)*, Sep. 2018, pp. P.1–P.10.

[51] A. Ghosh, A. Ukil, and A. P. Hu, "PV-battery system with wireless power transfer for LV applications," in *Proc. IECON 46th Annu. Conf. IEEE Ind. Electron. Soc.*, Oct. 2020, pp. 4283–4287.

[52] A. Ghosh, A. Ukil, and A. P. Hu, "Integration of rooftop solar PV generation with wireless power transfer," in *Proc. IEEE PES Asia–Pacific Power Energy Eng. Conf. (APPEEC)*, Dec. 2019, pp. 1–5.

[53] J. Zhu, T. U. K. Nutakki, P. K. Singh, B. S. Abdullaeva, X. Zhou, Y. Fouad, and L. H. Alzubaidi, "Sustainable off-grid residential heating and desalination: Integration of biomass boiler and solar energy with environmental impact analysis," *J. Building Eng.*, vol. 87, Jun. 2024, Art. no. 109035, doi: 10.1016/j.jobe.2024.109035.

[54] Y. Zheng, Z. Cheng, C. Liu, H. Liu, M. Amirabadi, and B. Lehman, "Modular wireless power transmission for photovoltaic subpanel system," in *Proc. IEEE Energy Convers. Congr. Expo. (ECCE)*, Vancouver, BC, Canada, Oct. 2021, pp. 546–553.

[55] M. Elwalaty, M. Jemli, and H. B. Azza, "A two-rectangular coils wireless charging electric vehicle with photovoltaic generator," in *Proc. 19th Int. Conf. Sci. Techn. Autom. Control Comput. Eng. (STA)*, Sousse, Tunisia, Mar. 2019, pp. 455–460.

[56] A. Shahin, J.-P. Martin, S. Pierfederici, and A. M. Sharaf, "Integration of renewable energy sources to wireless charger of electrical vehicle," in *Proc. 22nd IEEE Int. Conf. Ind. Technol. (ICIT)*, vol. 1, Valencia, Spain, Mar. 2021, pp. 397–402.

[57] S. Hiranuma, T. Takayanagi, N. Hoshi, J. Haruna, and M. Cao, "Experimental consideration on DC–DC converter circuits for fuel cell hybrid electric vehicle," in *Proc. IEEE Int. Electr. Vehicle Conf.*, Greenville, SC, USA, Mar. 2012, pp. 1–8, doi: 10.1109/IEVC.2012.6183264.

[58] P. S. Subudhi, S. Padmanaban, F. Blaabjerg, and D. P. Kothari, "Design and implementation of a PV-fed grid-integrated wireless electric vehicle battery charger present in a residential environment," *IEEE J. Emerg. Sel. Topics Ind. Electron.*, vol. 4, no. 1, pp. 78–86, Jan. 2023, doi: 10.1109/JESTIE.2022.3195087.

[59] X. Tan, S. Duan, and Y. Li, "A two-stage EV wireless charging system based on LCC-S resonance and its wide input and output voltage range control method," in *Proc. 26th Int. Conf. Electr. Mach. Syst. (ICEMS)*, Nov. 2023, pp. 5245–5250, doi: 10.1109/ICEMS59686.2023.10344536.
[60] R. Mai, Y. Chen, Y. Zhang, N. Yang, G. Cao, and Z. He, "Optimization of the passive components for an S-LCC topology-based WPT system for charging massive electric bicycles," *IEEE Trans. Ind. Electron.*, vol. 65, no. 7, pp. 5497–5508, Jul. 2018, doi: 10.1109/TIE.2017.2779437.
[61] Y. Zhou and B. Li, "Cascade control of wireless charging LCC-LCC structure based on ADRC," in *Proc. IEEE 7th Adv. Inf. Technol., Electron. Autom. Control Conf. (IAEAC)*, vol. 7, Mar. 2024, pp. 428–432, doi: 10.1109/IAEAC59436.2024.10503671.
[62] P. Zhang, M. Saeedifard, O. C. Onar, Q. Yang, and C. Cai, "A modular integration design of LCL circuit featuring field enhancement and misalignment tolerance for wireless EV charging," in *Proc. IEEE Appl. Power Electron. Conf. Expo. (APEC)*, New Orleans, LA, USA, Mar. 2020, pp. 1634–1640, doi: 10.1109/APEC39645.2020.9124333.

K. ARULVENDHAN received the M.E. degree in power electronics and drives from the Kumaraguru College of Technology. He is an Assistant Professor with the Department of Electrical and Electronics, SRM Institute of Science and Technology. Since 2013, he has been a vital part of the academic community, contributing significantly to research in charging systems for electric vehicles and electrical machines. His educational background enhances his role in shaping the next generation of engineers, aligning with the department's commitment to excellence in electrical and electronics engineering education and sustainable technologies.

SRINIVAS KANDADAI NAGARATNAM received the D.E.E.E. degree from the Chenkalvarayan Polytechnic, Chennai, in 1985, the M.E. degree in power systems from Annamalai University, in 1993, and the Ph.D. degree in electrical engineering from Anna University, in 2004. Currently, he is the HOD/EEE with SRM IST, Ramapuram Campus, Chennai. He has about 120 international journal and international conference publications. He received the AMIE certification from the Electrical Engineering Branch, I.E., India in 1989. He has authored three textbooks for engineering students on the fundamentals of electrical and electronics engineering. He has executed two funded projects from TNSCST and has completed a project on 3-D magnetic field sensor project for DRDO, an Indian government defense organization. His interests are power system contingency analysis, unit commitment and economic dispatch, modeling of electric drives and finite element analysis based electromagnetic and mechanical characterization of electrical machines—individually and for electric vehicle applications. He was a recipient of the IEEE Best Paper Awards in the IEEE International Conferences IECON 2000 which was held in Japan and IECON 2003 which was held in the USA.

R. NARAYANAMOORTHI received the bachelor's degree in electrical engineering and the master's degree in control and instrumentation from Anna University, India, in 2009 and 2011, respectively, and the Ph.D. degree from the SRM Institute of Science and Technology, India, in 2019. He is currently an Associate Professor with the Department of Electrical and Electronics Engineering, SRM Institute of Science and Technology. His research interests include wireless power transfer, electric vehicles, power electronics, artificial intelligence, machine learning in renewable energy systems, and embedded systems for smart sensors.

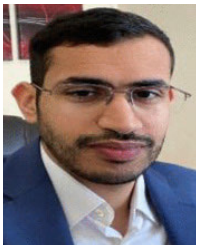

MOHAMMED ALHARBI received the B.S. degree in electrical engineering from King Saud University, Riyadh, Saudi Arabia, in 2010, the M.S. degree in electrical engineering from Missouri University of Science and Technology, Rolla, MO, USA, in 2014, and the Ph.D. degree in electrical engineering from North Carolina State University, Raleigh, NC, USA, in 2020. He was a Teaching Assistant with King Saud University, from September 2010 to May 2011. He was a Project Engineer with the FREEDM Systems Center, North Carolina State University, from January 2016 to December 2019, where he was involved in designing and constructing a modular multilevel converter for control validations. In August 2020, he joined the Department of Electrical Engineering, King Saud University, where he is currently an Assistant Professor. His research interests include medium-voltage and high-power converters, modular multilevel converter (MMC) controls, multi terminal HVDC systems, and grid integration of renewable energy systems.

SEADA HUSSEN was born in Wollo, Ethiopia, in 1992. She received the B.Sc. degree in electrical and computer engineering (power stream) from Haramaya University, in 2015, and the M.Sc. degree in power system engineering from Addis Ababa Science and Technology University, in 2020. She is currently pursuing the Ph.D. degree in electrical power engineering with Adama Science and Technology University. She is also with Haramaya University, as a Lecturer and a Researcher. She is serving as an editor and/or a reviewer for different international journals. She has published 23 research articles in reputable journals and conference publications.